Formation and decay of Xe $4d^{-1}$ vacancies studied via electron-electron coincidence experiments

L. Avaldi,[1] P. Bolognesi,[2] R. Camilloni,[1] E. Fainelli,[1] R. A. Multari,[1,*] and G. Stefani[3]
[1]*Istituto di Metodologie Avanzate Inorganiche del Consiglio Nazionale delle Ricerche, Area della Ricerca di Roma, Casella Postale 10,00016 Monterotondo, Italy*
[2]*Dipartimento di Fisica, Università di Roma ''La Sapienza,'' Piazza Aldo Moro 7, Roma, Italy*
[3]*Dipartimento di Fisica ''E. Amaldi'' and Istituto Nazionale di Fisica della Materia, Unità di Roma III, Università di Roma III, Roma, Italy*
(Received 18 August 1995; revised manuscript received 21 March 1996)

A versatile electron-impact spectrometer, equipped with three independent electrostatic analyzers, has allowed the simultaneous investigation of the excitation and ionization and Auger decay of the Xe $4d$ states via electron-electron coincidence experiments. Energy and angular dependence of the final-state continuum interactions, the postcollision interactions, has been studied in both the $(e,e'$ Auger) and $(e,2e)$ binding energy spectra up to 30 eV above the $4d$ thresholds. The experimental results have been compared with the theoretical predictions of Kuchiev and Sheinerman (Usp. Fiz. Nauk **158**, 353 (1989) [Sov. Phys. Usp. **32**, 569 (1989)]). A fairly good agreement between the experiments and theory has been found in all the studied cases. Also the decay of the Xe $4d^{-1}np$ inner-shell excited states and the energy dependence of the $4d_{5/2}$:$4d_{3/2}$ branching ratios have been studied and compared with analogous data from photoionization experiments. [S1050-2947(96)05909-4]

PACS number(s): 34.80.Dp, 32.80.Hd

I. INTRODUCTION

Since their introduction in late 1960s, electron-electron coincidence experiments have become a well established technique to study electron impact ionization of atoms and molecules [1,2]. A large body of experimental and theoretical work has been devoted to understand the mechanism of the ionization process itself and to single out features typical of the different interactions (binary electron-electron, electron-ion, exchange, and final-state interactions) that cause ionization [3]. It has been shown that whenever the momentum and energy transfer to the target are adsorbed by one electron the impulse approximation holds and within the single-particle approximation the coincidence cross section can be directly related to the momentum density of the ionized orbital [4]. On this ground is based electron momentum spectroscopy (EMS); the wave-function maps, which EMS provides, are nowadays one of the most sensitive tests for quantum chemistry calculations [5]. The electron-electron coincidence technique has then been extended to pinpoint more subtle processes where either the simultaneous ionization and excitation of the target occurs [6,7] or ionization proceeds via competitive direct and resonant channels [8]. All of this work has been focused on ionization of valence shells.

Inner-shell ionization is an even more interesting and, of course, complex process, because it results in an unstable singly charged ion, which may suffer radiative or nonradiative decays. Depending on the ionic state reached in the first decay step the process may continue further with a radiative-nonradiative cascade. Over the last few years it has become more and more evident that inner-shell hole creation and decay have to be treated as a single multiple-ionization process that proceeds from a common intermediate state along different pathways rather than a stepwise sequence of independent transitions. This is true as much the process occurs close to the ionization threshold. It is therefore evident that experiments with the simultaneous detection of as many as possible of the final charged products of the reaction are needed to gain full perspective of the evolution of a core state. Among the other coincidence techniques electron-electron coincidence experiments may play a leading role in this field because they allow the study of the different ionic states independently of the following fate of the multiply charged residual ion. However, after the pioneering work of Camilloni *et al.* on C $1s$ Ref. [9], the low cross section and the unfavorable true-to-random coincidence ratio have hampered the investigation of inner shells by $(e,2e)$ experiments for a long time. Recently, taking advantage of both the larger cross section obtainable in asymmetric kinematics and the increased efficiency of multichannel coincidence apparatuses, some coincidence studies of inner-shell ionization have been reported [10–17]. In these works either the two electrons produced in the primary ionization event or one of these electrons and the Auger electron ejected in the decay of the inner hole were detected in coincidence. In the present work we have modified our coincidence spectrometer by adding a third electron analyzer in order to study simultaneously the formation and decay of the inner hole via electron-electron coincidence experiments. The first studied case has been the ionization and decay of the Xe $4d$.

Xe $4d$ has often been used as a showcase for several characteristic features of atomic inner-shell excitation and ionization. These features display both one-electron character, directly invoking transitions of $4d$ electrons, for instance, the shape resonance, and many-electron character, for example, the interchannel coupling between the $5p$ and $5s$

*Present address: Chemical Science and Technology Dept., Los Alamos National Laboratory, CST2 MS J565, Los Alamos, New Mexico 87545.

outer shells and the Auger decay of the $4d$ vacancies. All these characteristics have been largely explored by photoexcitation and photoionization studies [18] and also the formation and decay of the Xe $4d$ hole has been studied to some extent in a photoelectron-photoelectron coincidence experiment by Okuyama, Eland, and Kimura [19]. In contrast data from electron-impact experiments are lacking [13]. Electron-impact experiments allow one to study the excitation and decay of dipole forbidden transitions, such as the $4d \rightarrow nd$ ($n \geqslant 5$) ones, as well as to investigate the dynamics of the excitation-ionization process at different momentum transfer **K**. Thus selecting collisions belonging to the dipolar regime, $K \rightarrow 0$, the collective interactions of the incident electron with the target atom are investigated, while the role of the two-body interactions can be studied in events at larger K, i.e., in the impulsive regime.

In the present study the Xe $4d$ ionization has been studied at about 1000-eV incident energy and for several values of the energy loss ΔE from 65.1 eV, which corresponds to the $4d_{5/2} \rightarrow 6p$ transition energy [20] up to 97.5 eV, i.e., 30 eV above the $4d_{5/2}$ ionization threshold. The experiment below the $4d$ ionization thresholds addresses the resonant Auger processes [21], while the full body of the other experiments represents a complete investigation of the postcollision interactions, PCI [22], among the three unbound electrons present in the final state of the reaction

$$e(E_0) + \mathrm{Xe} \rightarrow \mathrm{Xe}^{+}(4d^{-1}) + e_a(E_a) + e_b(E_b) \downarrow \mathrm{Xe}^{2+} + e_A(N_{45}O_{23}O_{23}). \quad (1)$$

While the energy dependence of PCI has attracted a lot of experimental work, less attention has been paid to the angular dependence [17,23]. In the previous electron-impact studies [14–16,24] the fast scattered and Auger electrons have been measured in coincidence. Therefore the PCI effects have been averaged over all the directions of the slow ejected electrons. Only Kammerling, Krassig, and Schmidt [25] in a photoionization experiment and Sarkady *et al.* [26] in a non-coincidence ion-atom collision experiment attempted a direct measurement of the PCI angular dependence.

Here we have completed the investigation of PCI effects by detecting in coincidence the slow ejected electron and the Auger electron from the transition $N_5O_{23}O_{23}$ ($^1S_0$) at different relative emission angles. Care has been taken to select a kinetic energy E_b close to that of the Auger electron in order to maximize the energy and momentum exchange between the two electrons. A brief report of this latter experiment has been already presented elsewhere [27].

To our knowledge this is the first experiment where the formation and decay of an inner shell are studied simultaneously and where the resonant Auger process is addressed

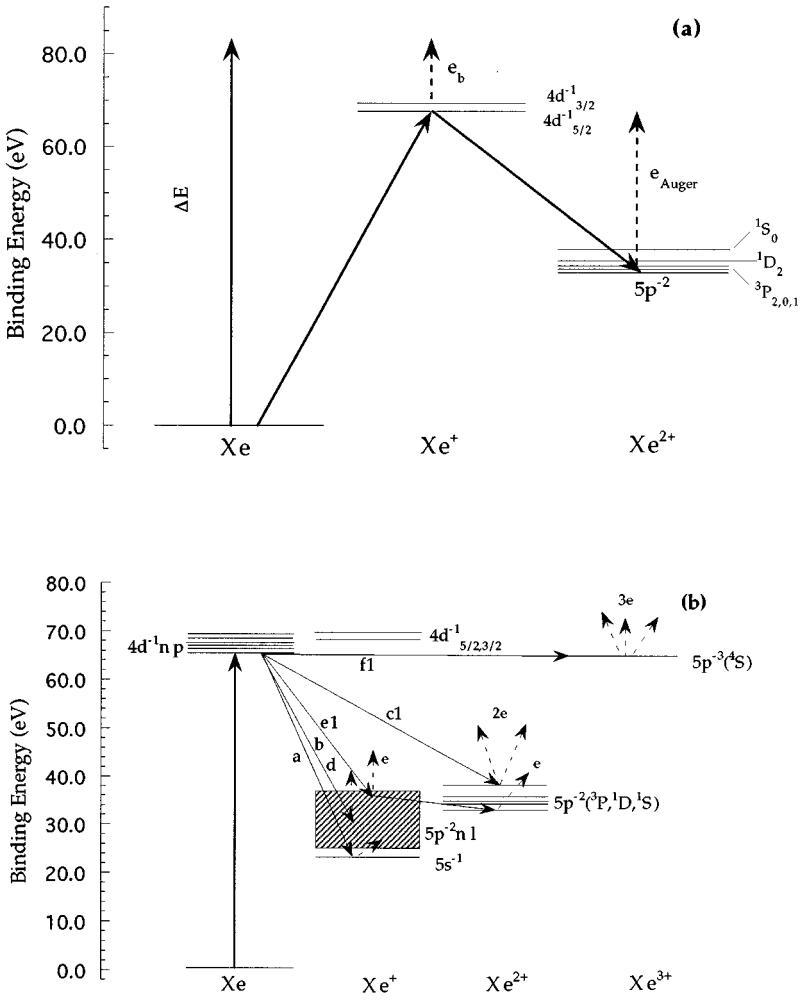

FIG. 1. (a) Schematic diagram of the ionization and decay of $4d$ states. Only the three lowest Xe^{2+} states are shown. (b) Schematic diagram of the excitation of a $4d^{-1}nl$ state and its decay. The dashed area indicates the manifold of the Xe^{+} $5p^4nl$ states. The same labels of the text are used to indicate the different decay routes of the inner-shell excited state.

in an electron-impact experiment. The paper is organized as follows. In the next section, as a background for the present work, a brief summary of the main processes occurring when the Xe atom is excited or ionized in the energy region near the $4d$ threshold is given. Then in Sec. III the experimental setup and the procedures used in the measurements are described. Sections IV and V are devoted to the experimental results and their discussions. Finally some remarks and conclusions are presented in Sec. VI.

II. SCHEMATICS OF THE PROCESSES NEAR THE 4*d* IONIZATION THRESHOLDS

A sketch of the spectroscopy and dynamics of the states involved in the excitation or ionization of Xe in the energy region near the $4d$ thresholds is shown in Fig. 1, while the energies of the main transitions and ionic states involved are reported in Table I.

At energy losses ΔE larger than the $4d$ binding energies (67.5 and 69.5 eV for the $4d_{5/2}$ and $4d_{3/2}$ states, respectively) direct ionization of the $4d$ states occurs:

$$\begin{aligned} e(E_0)+\mathrm{Xe}&\rightarrow \mathrm{Xe}^+(4d^9 5s^2 5p^6)+e_a(E_a)+e_b(E_b) \\ &\downarrow \\ &\mathrm{Xe}^{2+}+e_A(N_{45}OO) \end{aligned} \tag{2}$$

and then the inner-shell hole mainly decays to the Xe^{2+} energetically accessible states via an Auger decay [Fig. 1(a)]. Direct double ionization as well as triple ionization [28] processes, energetically allowed, represent a negligible fraction of the total cross section in this energy region.

At ΔE smaller than the $4d$ binding energies a $4d$ electron can be promoted to one of the unoccupied states np $(n\geqslant 6)$, nd $(n\geqslant 5)$ via the process

$$e(E_0)+\mathrm{Xe}\rightarrow \mathrm{Xe}^*(4d^9 5s^2 5p^6 nl)+e_a(E_a=E_0-\Delta E_{nl}), \quad l=p,d, \tag{3}$$

where the energy loss suffered by the incident electron is equal to the $4d\rightarrow nl$ transition energy [Fig. 1(b)].

The inner-shell excited states $\mathrm{Xe}^*(4d^9 np)$ may decay via the following paths:

$$\begin{aligned} \mathrm{Xe}4d^9 5s^2 5p^6(^2D)np\ ^1P_1 &\rightarrow \mathrm{Xe}^+ 4d^{10} 5s^2 5p^5(^2P)+e && \text{(a1)}, \\ &\mathrm{Xe}^+ 4d^{10} 5s^1 5p^6(^2S)+e && \text{(a2)}, \\ &\mathrm{Xe}^+ 4d^{10} 5s^2 5p^4(^1D)nd(^2S)+e && \text{(b1)}, \\ &\mathrm{Xe}^+ 4d^{10} 5s^2 5p^4(^1D)ns(^2S)+e && \text{(b2)}, \\ &\mathrm{Xe}^{2+} 4d^{10} 5s^2 5p^4(^3P,^1S,^1D)+2e && \text{(c1)}, \\ &\mathrm{Xe}^+ 4d^{10} 5s^2 5p^4(^SL_J)np+e && \text{(d1)}, \\ &\mathrm{Xe}^+ 4d^{10} 5s^1 5p^5(^SL_J)np+e, && \text{(d2)}, \\ &\mathrm{Xe}^+ 4d^{10} 5s^2 5p^4(^SL_J)n'p+e \quad n'>n && \text{(d3)}, \\ &\mathrm{Xe}^+ 4d^{10} 5s^2 5p^4(^SL_J)n'p+e\rightarrow \mathrm{Xe}^2+4d^{10} 5s^2 5p^4(^SL_J) && \text{(e1)}, \\ &\mathrm{Xe}^{3+} 4d^{10} 5s^2 5p^3(^4S)+3e && \text{(f1)}, \end{aligned} \tag{4}$$

TABLE I. Energies of the main transitions and ionic states involved in the excitation and ionization and decay of the Xe $4d$ states. The binding energies of the Xe^+ $5p^4 nl$ states involved in the decay of the $4d^{-1}nl$ inner-shell excited states are not reported. A complete list of these states can be derived from Tables I of Refs. [38] and [39].

State	$4d_{5/2}^{-1}$	$d_{3/2}^{-1}$
(a) Xe excited states near the $4d$ ionization thresholds (Ref. [20])		
$4d^{-1}6p$	65.110	67.039
$4d^{-1}5d$	65.446	67.411
$4d^{-1}7p$	66.375	68.345
$4d^{-1}8p$	66.854	68.838
(b) Xe^+ states		
$5p_{3/2}^{-1}$	12.129	
$5p_{1/2}^{-1}$	13.436	
$5s^{-1}$	23.397 (Ref. [57])	
$4d_{5/2}^{-1}$	67.548 (Ref. [20])	
$4d_{3/2}^{-1}$	69.537 (Ref. [20])	
(c) Xe^{2+} states (Refs. [57] and [58])		
$5p^{-2}(^3P_2)$	33.08	
$5p^{-2}(^3P_0)$	34.09	
$5p^{-2}(^3P_1)$	34.29	
$5p^{-2}(^1D_2)$	35.20	
$5p^{-2}(^1S_0)$	37.56	
$5s^{-1}5p^{-1}(^3P_2)$	45.26	
$5s^{-1}5p^{-1}(^3P_0)$	45.92	
$5s^{-1}5p^{-1}(^3P_1)$	46.65	
$5s^{-1}5p^{-1}(^1P_0)$	47.84	
(d) Xe^{3+} state		
$5p^{-3}(^4S)$	64.4 (Ref. [28])	

where processes (a) represent direct recombination, processes (b) the autoionization to satellite states, (c1) is direct shakeoff to doubly charged ions, and finally processes (d) are the resonant Auger decays. In this latter process the electron in the excited state either remains as a spectator of an Auger process involving the outer shells and the $4d$ hole (d1,d2) or participates in the process, which ends up in a configuration Xe^+ $(5p^4n'l)$ with $n'>n$ (d3). The processes in which the np electron acts as a spectator end up with Auger lines built on the same Xe^{2+} parent states, but shifted up in energy due to the $5p$-np coupling energy. For example in the case of a $6p$ spectator electron the Auger lines relative to the Xe^{2+} ^3P, ^1D, and ^1S core states occur in the energy region above 36.4 eV. In the case of the shakeup transitions (d3) the Auger lines occur at lower energy than in the previous case due to the energy needed to promote the excited electron to an outer orbital. Processes (e1) are two-step decay where a doubly charged ion is formed via the resonant Auger decay followed by autoionization [29,30]. Finally the decay to Xe^{3+} with the simultaneous emission of three electrons (f1) is also energetically allowed.

Photoionization experiments have shown [21,19] that the processes (a)+(b) account for about 13% of the total decay and the decay to Xe^{3+} for about 0.5%. The probability of a decay to stable neutral Xe via fluorescence is unknown, but certainly small according the measured yield of Xe^+, Xe^{2+}, and Xe^{3+} ions and the absolute absorption and ionization cross sections [18,21]. Thus the main decay routes are the direct shakeoff of two electrons and the resonant Auger process.

The transitions $Xe \rightarrow Xe^* 4d^9 nd (n \geq 5)$ are dipole forbidden and they can be studied only in the electron-impact experiments [20]. No information exists on the decay routes of these inner-shell excited states.

III. EXPERIMENT

The apparatus for the present electron-electron coincidence measurements is an electron-impact spectrometer specially designed for coincidence experiments [13,31]. In these measurements the spectrometer has been modified and a third electrostatic analyzer has been added. Details of the setup have been reported elsewhere [13,31] thus only a brief description will be given here. The attention will be focused on the new analyzer and the measurements that it enables.

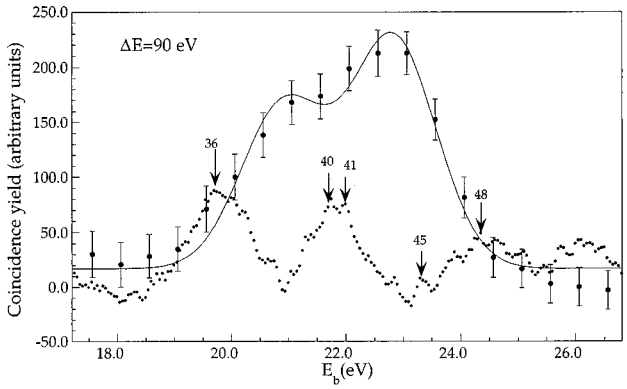

FIG. 2. $(e,2e)$ binding energy spectrum (dots with the error bars) of the Xe $4d$ orbitals vs the ejected electron energy E_b measured at $\Delta E = 90$ eV. The Auger spectrum (small dots) measured during the coincidence run by the ejected electron analyzer and overimposed to the coincidence spectrum in the figure is used to determine the energy scale The peaks in the noncoincidence spectrum are labeled according to Ref. [32].

The electron beam, formed by a modified Varian glancing electron gun, crosses an effusive beam in the center of the vacuum chamber. The density at the electron-gas-beam crossing point can be as high as 5×10^{12} mol/cm^3, which means a local pressure approximately a few hundred times larger than the background pressure. The outgoing electrons are collected by two twin hemispherical electrostatic analyzers independently rotatable in the scattering plane ($-15°$/150° with respect to the incident beam direction) and the

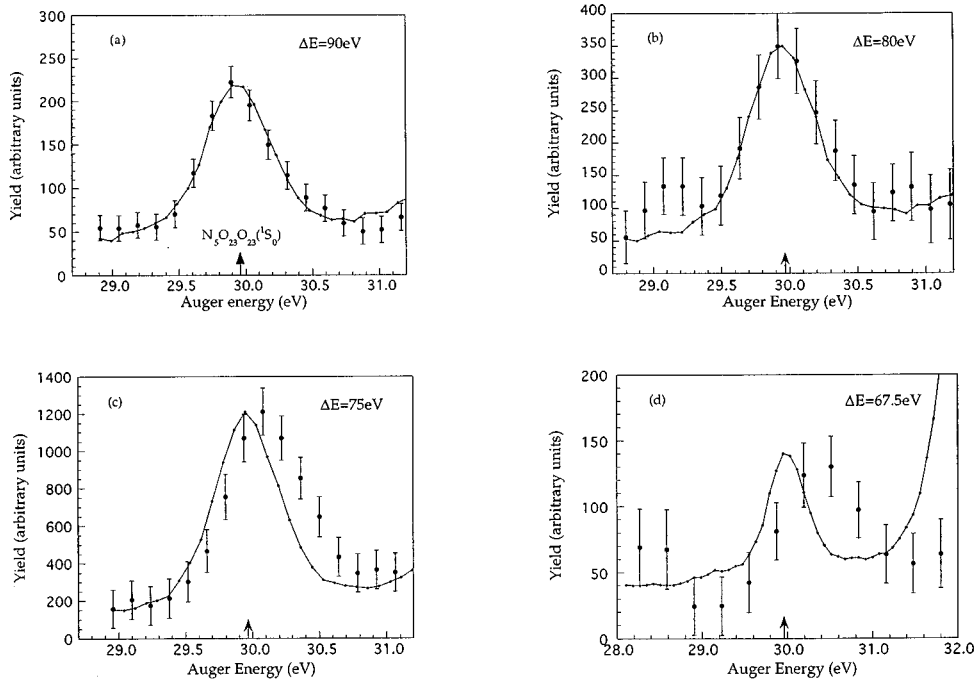

FIG. 3. Xe $N_5O_{23}O_{23}(^1S_0)$ (e,e') Auger) spectra measured at $\Delta E = 90$ eV (a), 80 (b), 75 (c), and 67.5 eV (d). The full line is the noncoincidence Auger yield recorded by the CMA during the coincidence measurements.

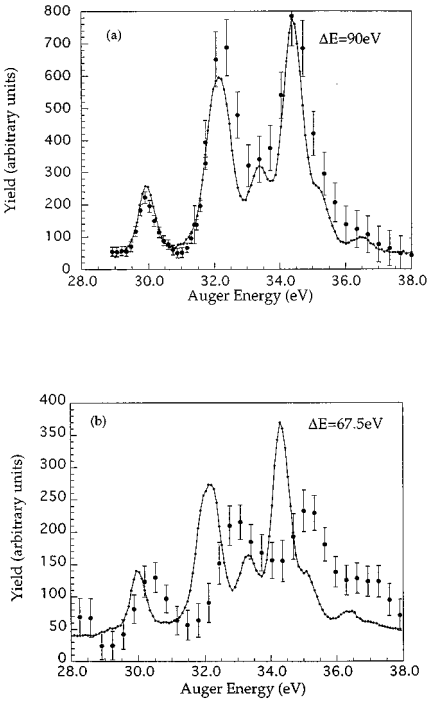

FIG. 4. Xe $N_{45}O_{23}O_{23}$ (e,e' Auger) spectra measured at ΔE =90 eV (a) and 67.5 eV (b). The full line is the noncoincidence Auger yield recorded by the CMA during the coincidence measurements.

new cylindrical mirror analyzer (CMA), located perpendicularly to the scattering plane.

The hemispherical analyzers are formed by a decelerating three-element zoom lens followed by a hemispherical electrostatic deflector (105 and 135 mm inside and outside diameter, respectively). The angular acceptances of the analyzers in the present measurements were set to $\pm 0.5°$ and $\pm 2°$ for the scattered and ejected electron analyzer, respectively.

The CMA is a Riber OPC104, with an exit slit suitably modified to have a field of view large enough to include the interaction region and to overlap the field of view of the other two analyzers. In the present configuration the CMA has a resolving power $E/\Delta E \approx 50$, which enables it to collect the Xe $N_{45}O_{23}O_{23}$ Auger lines ($29 \leqslant E_A \leqslant 35$) with a resolution of about 650 meV. The analyzer is perpendicular to the scattering plane and the effusive gas beam is obtained by letting the gas through a needle set internally to and coaxial with the inner cylinder of the CMA. The tip of the needle is gold and is placed about 1.5 mm below the electron-beam path. It has been insulated from the rest of the gas inlet fixture to provide a monitor of the stability of the electron beam at the scattering center during the long coincidence runs.

Being equipped with three independent analyzers the spectrometer enables us to perform simultaneously several experiments. In the noncoincidence mode of operation while one hemispherical analyzer collects an energy-loss spectrum the other one can be rotated around the scattering center measuring the angular distribution of ejected electrons of fixed energy. At the same time the CMA can collect an Auger spectrum whenever the incident electron energy is high

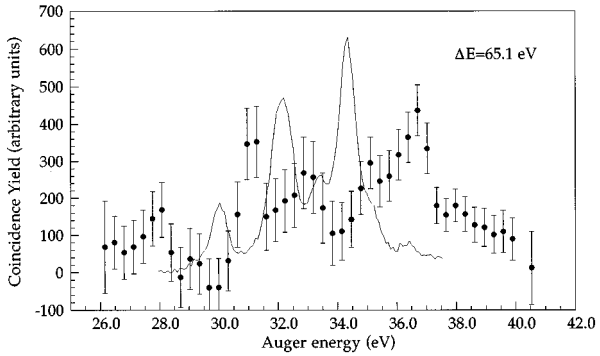

FIG. 5. Xe (e,e' Auger) spectra measured at $\Delta E = 65.1$ eV, compared with the noncoincidence spectrum (full line) measured by the CMA during the coincidence experiment.

enough to produce inner-shell ionization. In the coincidence operation mode ($e,2e$) and (e,e' Auger) measurements can be performed simultaneously, collecting the pair of electrons of the primary ionization events with the two hemispherical analyzers and the pair formed by one of them and the Auger electron with one hemispherical analyzer and the CMA.

In order to perform multicoincidence experiments we have replaced the time-to-amplitude converter (TAC) of our coincidence electronics with a time-to-digit converter (TDC) (LeCroy 4208). This quite versatile CAMAC unit enables the reading of up to eight independent events with respect to the same common start. The TDC as well as all the other CAMAC units (counters, analog-to-digital, and digital-to-analog converters) are governed by a DSP 6002 crate controller via a 486 personal computer.

In all the present measurements the scattered electron energy E_a has been fixed at 1000 eV and the scattered electrons have been always detected at 4° with respect to the incident beam direction. Several values of the ejected electron energy E_b in the range 5 to 30 eV have been used. The energy resolution in both the hemispherical analyzers is $\Delta E_a = \Delta E_b = 1.1$ eV full width at half maximum (FWHM). This results in a coincidence energy resolution $\Delta E_c = (\Delta E_a^2 + \Delta E_b^2)^{1/2} = 1.6$ eV FWHM in the binding energy spectra. In the (e,e' Auger) measurements the energy resolution is determined by the Auger channel, i.e., by the energy resolution of the CMA that has been measured to be ≈ 650 meV in the energy region of the Xe $N_{45}O_{23}O_{23}$ Auger spectrum.

In the simultaneous measurement of the two coincidence spectra the following procedure has been used. At each selected ΔE the incident energy E_0 was fixed in order to have $E_0 - \Delta E = E_a = 1000$ eV and then both the ejected and Auger electron energies were scanned. While this is the usual procedure for (e,e' Auger) measurements, it is quite unconventional in measuring ($e,2e$) energy spectra. The usual way consists in fixing the kinetic energies of the two detected electrons and then scanning E_0. A coincidence peak will be detected only at $E_0 - (E_a + E_b) = \varepsilon_{nl}$ where ε_{nl} is the ionization potential of an ionic state. By this procedure all the ionic states in the spectrum are excited at the same energy above their respective thresholds. On the contrary, the procedure used in this work, where ΔE is fixed, is equivalent to a photoionization experiment at a fixed photon energy $h\nu = \Delta E$. Thus the different ionic states being excited at differ-

ent energies above their respective thresholds produce ejected electrons with different kinetic energies.

One of the main effects of PCI is the energy shift of the Auger and ionic peaks in the $(e,e'$ Auger) and $(e,2e)$ energy spectra, respectively. In order to evaluate this shift and to make a comparison with the theoretical predictions (see Sec. V) an energy scale has to be established in both the coincidence spectra. In the case of the $(e,e'$ Auger) measurements the energy scale is established relative to the noncoincidence spectrum measured by the CMA (see Figs. 3 and 4) during the coincidence experiment. For the $(e,2e)$ binding energy spectra we have used a similar procedure. Indeed the Xe $N_{45}OO$ Auger spectrum, which involves the $4d^9 \rightarrow 5s^0 5p^6$, $5s^1 5p^5$, and $5s^2 5p^4$ transitions, extends from 5.87 to 36.44 eV [32]. Thus using the noncoincidence electron yield measured during the coincidence run and more detailed spectra collected with 100 meV per step before and after each coincidence run has made it possible to put the $(e,2e)$ binding energy spectra on a relative energy scale. As an example in Fig. 2 is shown the $(e,2e)$ spectrum at $\Delta E = 90$ eV, together with the noncoincidence spectrum measured by the slow ejected electron analyzer. The noncoincidence spectrum shown is obtained after the subtraction of the background of the secondary electrons, represented by a fourth degree polynomial, and is a small fraction ($\approx 10\%$) of the measured electron yield. The peaks due to the $N_{45}O_1O_{2,3}$ (^1P) and ($^3P_0$) transitions are clearly seen. All the features in Fig. 2 can be assigned according the Xe NOO spectrum measured by Aksela, Aksela, and Pulkkinem [32] and the numbering reported on the main features in the figure refers to that work. These features have been used to calibrate the energy scale of the $(e,2e)$ binding energy spectrum.

The typical coincidence count rate was between 0.1 and 0.01 s^{-1}, while the true-to-random ratio was never better than 1/5. The accumulation time in the worst case (study of the angular dependence of PCI) was about 14 h per point. Due to these long accumulation times accurate tests of the stability of the spectrometer have been done by measuring the coincidence yield for the ionization of He $1s$ in asymmetric conditions ($E_a = 600$ eV, $E_b = 40$ eV, $\vartheta_a = 4°$, and $\vartheta_b = 60°$) daily for a full month and the coincidence yield for the ionization of the Xe $5p$ orbital in asymmetric kinematics ($E_a = 1000$ eV, $E_b = 56$ eV, $\vartheta_a = 4°$, and $\vartheta_b = 260°$) simultaneously to one of the $(e,e'$ Auger). Despite the quite different coincidence rate in the two tests, 2.5 ± 0.04 and 0.05 ± 0.007 s^{-1} for the He and Xe measurements, respectively, the data were distributed within the statistical uncertainties and well represented by a normal distribution.

IV. EXPERIMENTAL RESULTS

A. (e,e' Auger) coincidence spectra

The decay of the $4d$ hole has been studied at a few ΔE values, namely, 67.5, 75, 80, and 90 ± 1.1 eV by $(e,e'$ Auger) coincidence experiments. With ionization potentials of 67.5 and 69.5 eV for the $4d_{5/2,3/2}$ states, these ΔE correspond to ejected electron energies E_b between 0 and 22 eV. The coincidence $N_5O_{23}O_{23}(^1S_0)$ Auger lines at different ΔE are reported in Figs. 3(a)–3(d), while in Figs. 4(a) and 4(b) shown the full $N_{45}O_{23}O_{23}$ coincidence spectra collected at the two extreme ΔE values. The noncoincidence Auger spectrum, measured by the CMA during the coincidence scan, is also shown in each figure. This latter spectrum allows one to establish the energy scale and to evaluate the energy shifts and the distortions of the coincidence spectrum. We observe an almost complete overlap of the noncoincidence and coincidence spectra at $E_b = 20$ eV, [Fig. 3(a)] and then a progressive displacement of the coincidence spectrum towards higher kinetic energies as E_b decreases. At $\Delta E = 67.5$ eV [Fig. 4(b)] the difference is made even more dramatic by the absence of the $N_4O_{23}O_{23}$ components in the coincidence spectrum. The shift in the case of the $N_5O_{23}O_{23}(^1S_0)$ Auger line varies from 0.02 ± 0.1 to 0.45 ± 0.1 eV at $\Delta E = 90$ and 67.5 eV, respectively.

Another coincidence measurement has been then performed at $\Delta E = 65.1$ eV (Fig. 5), which corresponds to the Xe*$(4d^9 6p)$ excitation energy [20]. This latter experiment is meant to investigate the resonant Auger process. As in the previous figures, in Fig. 5 the noncoincidence Auger yield measured by the CMA during the coincidence scan has been overimposed to the coincidence spectrum. The comparison of the two spectra proves that any contribution of the $N_{45}O_{23}O_{23}$ Auger diagrammatic transitions to the coincidence spectrum can be excluded. Thus the measured spectrum will be interpreted in Sec. V A 2 in terms of resonant Auger transitions.

Finally in Fig. 6 are shown the results of the measurements where the ejected and Auger electrons in the final state of the reaction

$$\begin{aligned} & e(E_0 = 1000 \text{ eV}) + \text{Xe} \rightarrow \text{Xe}^+(4d_{5/2}^{-1}) + e_a(E_a = 902.5 \text{ eV}) + e_b(E_b = 30.0 \text{ eV}) \\ & \qquad \downarrow \\ & \qquad \text{Xe}^{2+}(5s^2 5p^4\ {}^1S_0) + e_A(29.95 \text{ eV}) \end{aligned} \tag{5}$$

are detected in coincidence. The measurements are performed at two different relative emission angles ϑ_{bA}, 25° and 170°, respectively. The energy of the ejected electron has been chosen to be 30 eV, i.e., close to that of the $N_5O_{23}O_{23}(^1S_0)$ Auger electron in order to maximize the interaction time and therefore the energy and momentum exchange between the two emerging particles. In the figures the ejected-Auger coincidence spectra are shown together with the noncoincidence Auger spectra (dashed line in the figures), simultaneously measured during the experiment. The noncoincidence yield has been scaled to the coincidence one, after a subtraction of a constant background. The coincidence spectrum taken at $\vartheta_{bA} = 170°$ is slightly shifted towards higher energy with respect to the noncoincident one

[Fig. 6(b)], while the one at $\vartheta_{bA}=25°$ [Fig. 6(a)] is clearly shifted towards low electron energies. A shift in this direction is consistent with the prediction of nonisotropic PCI theories [33–35], when the PCI inducer and the Auger electrons emerge with a small relative angle.

It is to be noted that all the measured coincidence $N_{45}O_{23}O_{23}$ spectra are overimposed to a continuum contribution due to direct double ionization events, where the third electron remains undetected. From the measurements of Fig. 6 an upper limit of $\cong 0.01$ Hz rate can be estimated for such a process. This figure prevents, at least in the present experimental conditions, the study of the direct double ionization process via an $(e,3e)$ experiment, where also the third electron is detected.

B. $(e,2e)$ binding energy spectra

The $(e,2e)$ binding energy spectra measured at $\Delta E=90$, 80, and 75 eV, simultaneously to the $(e,e'$ Auger) spectra described above, are shown in Figs. 7(a)–7(c) respectively. In these experiments the ejected electrons have been always detected at 260° with respect to the incident beam direction. In each figure the expected positions of the $4d^{-1}$ ionic states on the E_b scale are indicated by arrows. The most striking feature in these spectra is the change of the shape of the spectra at the different ΔE. A trial function with two Gaussians characterized by the same full width half maximum (FWHM) has been fitted to the experiments. The free parameters of the trial functions were, apart from the FWHM, the position of the $4d_{5/2}^{-1}$ ionic state and the branching ratio of the two spin-orbit components. The results show a large variation of the $4d_{5/2}$:$4d_{3/2}$ branching ratio. This ratio is 1.39 ± 0.17 at 90 eV, then decreases to 1.08 ± 0.14 at 80 eV, and finally suffers a large increase, up to a value larger than 3, at 75 eV. We can exclude that the $N_{45}OO$ Auger transitions occurring in the investigated E_b range make a contribution to the coincidence yield. First of all, as already mentioned in Sec. IV, the Auger yield represents a small fraction of the total electron yield measured at these energies, then a vanishing coincidence yield is measured, for example, at 14.2 eV, Fig. 7(b), where the stronger feature belonging to the $N_5O_1O_{23}$ manifold is observed in the ejected electron spectrum. Finally the agreement between the branching ratios of this $(e,2e)$ experiment and the ones from the photoionization experiments (Fig. 15), as discussed in Sec. V, confirms that in the present measurements the contribution of Auger transitions to the coincidence yield, if any, does not perturb the measured ratio.

The other observation in the $(e,2e)$ binding energy spectra is the shift of the ionic peaks towards lower ejected energies, as if the binding energy of the ionic state were larger, and a broadening of the peaks when ΔE approaches the $4d$ ionization thresholds. These effects are clearly seen in the spectrum at $\Delta E=75$ eV where the centroids of the $4d_{5/2}$ and $4d_{3/2}$ are shifted by about 0.43 ± 0.3 eV towards lower E_b and the FWHM of the peaks obtained in the fitting procedure is about 20% larger than the expected value according the energy resolution of the spectrometer. At $\Delta E=80$ eV the shift, if any, is 0.1 ± 0.09 eV, while at $\Delta E=90$ eV no shift has been detected within the present accuracy. In both cases the best fit results in a FWHM almost indistinguishable from the one expected from the energy resolution of the spectrometer.

Despite the large uncertainty, the shift observed in the $(e,2e)$ binding spectrum at $\Delta E=75$ eV is larger than the one

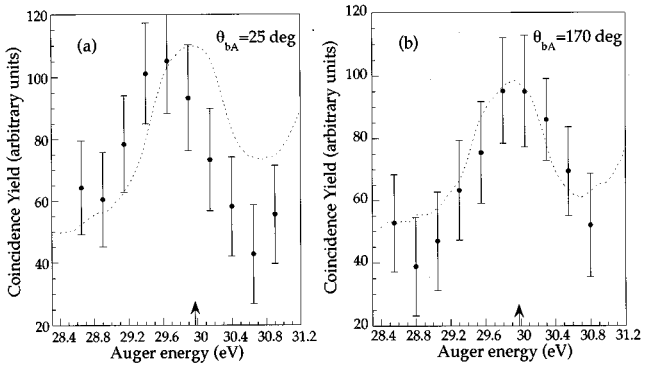

FIG. 6. Coincidence (dots) and noncoincidence (dashed line) spectra of the Xe $N_5O_{23}O_{23}(^1S_0)$ Auger line at 1000 eV incident energy and $\vartheta_{bA}=25°$ ($\vartheta_b=15°$ and $\vartheta_A=40°$) (a) and 170° ($\vartheta_b=260°$ and $\vartheta_A=90°$) (b).

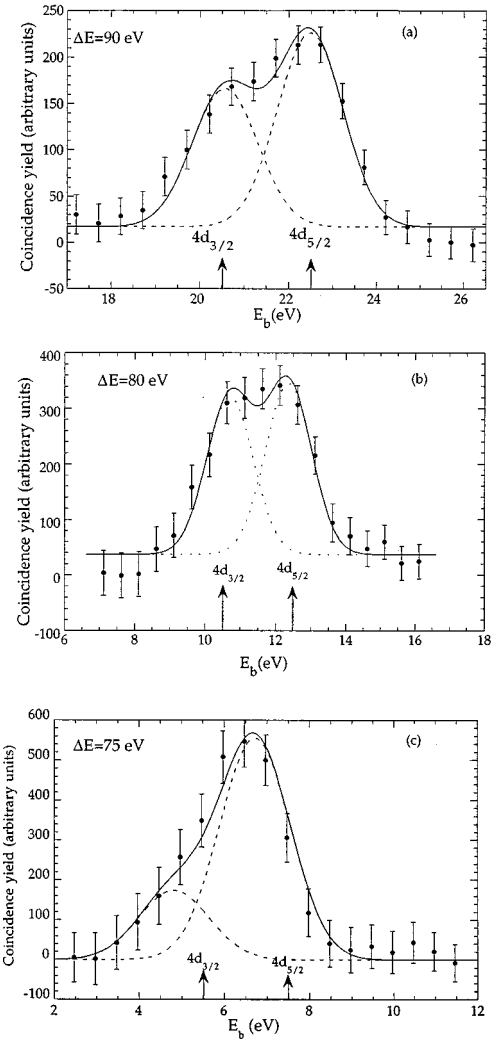

FIG. 7. Xe $4d$ $(e,2e)$ binding spectra measured at $\Delta E=90$ eV (a), 80 (b), 75 eV (c). The full line is a two Gaussian function fitted to the experiments, while the dashed lines are the contributions of the two spin-orbit components.

(0.14±0.1 eV) measured in the simultaneous (e,e') Auger). The different energy resolution of the two experiments, which affects the measured shift through the convolution of the natural linewidth with the experimental response function, cannot account for this difference. This might result from the PCI interaction, which here involves the slow ejected electron and all the Auger electrons of the NOO manifold, while in the $(e,e'$ Auger) measurement the PCI effects are due only to the interaction of one selected Auger electron and the slow ejected electron.

V. DISCUSSION

A. PCI effects

1. The model

The main observations in these coincidence experiments are the shift and asymmetric broadening of the Auger and ionic peaks when ΔE approaches the $4d$ thresholds. The final-state interaction, known as PCI between the ejected and Auger electrons is responsible for these observations. Among the several PCI theories proposed in the last years [33–36], which have shown in several cases similar accord with the experiments, we have chosen to compare the present results with the one by Kuchiev and Sheinerman [34] because this model is the only one that accounts for more than two interacting particles.

Kuchiev and Sheinerman [34] have derived the solution of the PCI problem in the case of reaction (1) within the eikonal approach. The hypothesis of this derivation is ''(i) the potential energies of interaction between e_a and e_b with the ion and with the Auger electron are less than the kinetic energies of the electrons and (ii) the electrons travel almost uniformly and rectilinearly at large distance'' [34]. The latter assumption implies that the relative angle does not change from the interaction region to the detector at infinity; i.e., the unbound electrons are assumed to travel along rectilinear trajectories. According to this model the cross section for the process (1) is given by

$$\frac{d^8\sigma}{dE_a dE_A d\Omega_a d\Omega_b d\Omega_A} = \frac{d^5\sigma}{dE_a d\Omega_a d\Omega_b} f(\Omega_A) \times l(E_A,\vartheta_{aA},\vartheta_{bA}), \tag{6}$$

where $f(\Omega_A)$ is the angular distribution of the Auger electrons and the PCI distorted line shape is given by

$$l(E_A,\vartheta_{aA},\vartheta_{bA}) = \frac{\Gamma/2\pi}{(E_A^0-E_A)^2+\Gamma^2/4}\, k(E_A,\xi) \tag{7}$$

with

$$k(E_A,\xi) = \frac{\pi\xi}{\sinh(\pi\xi)} \exp\left[2\xi \tan^{-1}\frac{2(E_A^0-E_A)}{\Gamma}\right] \tag{8}$$

and ξ given by

$$\xi = -\frac{1}{K_a} + \frac{1}{|\mathbf{K}_a-\mathbf{K}_A|} - \frac{1}{K_b} + \frac{1}{|\mathbf{K}_b-\mathbf{K}_A|}. \tag{9}$$

E_A^0 in (7) and (8) is the diagrammatic kinetic energy of the Auger electron, i.e., the energy difference between the one-hole and two-hole ion states. Due to hypothesis (ii) the time dependence of the momenta $\mathbf{K}_i (i=a,b,A)$ is neglected and the constant asymptotic values are used in (9).

The eightfold cross section (6) can be determined only by an experiment in which all three unbound electrons are detected in coincidence. In our actual measurements, where only the scattered or ejected and Auger electrons are detected in coincidence, the quantities that are measured are the sixfold cross sections

$$\frac{d^6\sigma}{dE_a d\Omega_a d\Omega_A dE_A} = \int d\Omega_b \frac{d^8\sigma}{dE_a d\Omega_a d\Omega_b d\Omega_A dE_A}, \tag{10a}$$

$$\frac{d^6\sigma}{dE_b d\Omega_b d\Omega_A dE_A} = \int d\Omega_a \frac{d^8\sigma}{dE_b d\Omega_a d\Omega_b d\Omega_A dE_A}, \tag{10b}$$

i.e., the cross section (6) integrated over all the directions either of the slow ejected electron (10a) or of the fast scattered electron (10b). The calculation of (10) implies the knowledge of the triple coincidence angular distribution of the ejected, scattered, and Auger electrons that at present is unknown. The triple coincidence angular distribution may be replaced, in (10a) for example, by the product of the $(e,2e)$ cross section for the ionization of the Xe $4d_{5/2}$ orbital, $d^5\sigma/d\Omega_a d\Omega_b dE_a$, and the angular distribution of the Xe $N_5O_{23}O_{23}(^1S_0)$ Auger electrons, $f(\Omega_A)$. Kuchiev and Sheinerman [34] instead suggested that the integration can be replaced by the calculation of (6) with the parameter ξ averaged over the solid angle of the undetected electron. Here this recipe has been adopted for the following reasons.

(i) In the scattered-Auger electron coincidence experiments the Auger yield, being measured by the CMA, is integrated over ±4° in the φ_A angle, i.e., the angle out of the scattering plane, and over 2π in ϑ_A the angle in the scattering plane. Therefore the observed PCI effects are averaged over the full angular distribution of the ejected electrons.

(ii) In the ejected-Auger electron coincidence experiments the unobserved particle is ≅6 times faster than the observed ones and mainly scattered in the forward direction [37]. Therefore its effect as a PCI inducer is expected to be negligible and the change in the line shape due to the choice of a ξ value averaged over Ω_a, if any, is not observable with the present experimental energy resolution.

2. (e,e′ Auger) experiments: PCI energy dependence and resonant Auger

In Fig. 8 the coincidence $N_5O_{23}O_{23}(^1S_0)$ Auger yields are compared with the theoretical predictions convoluted with the Gaussian response of the spectrometer. Analogous comparison is shown in Fig. 9 for the two complete $N_{45}O_{23}O_{23}$ spectra. The energy positions and the relative intensities of the different transitions belonging to the NOO manifold have been taken from Aksela, Aksela, and Pulkkinem [32]. The value of 111 meV, derived from the high-resolution

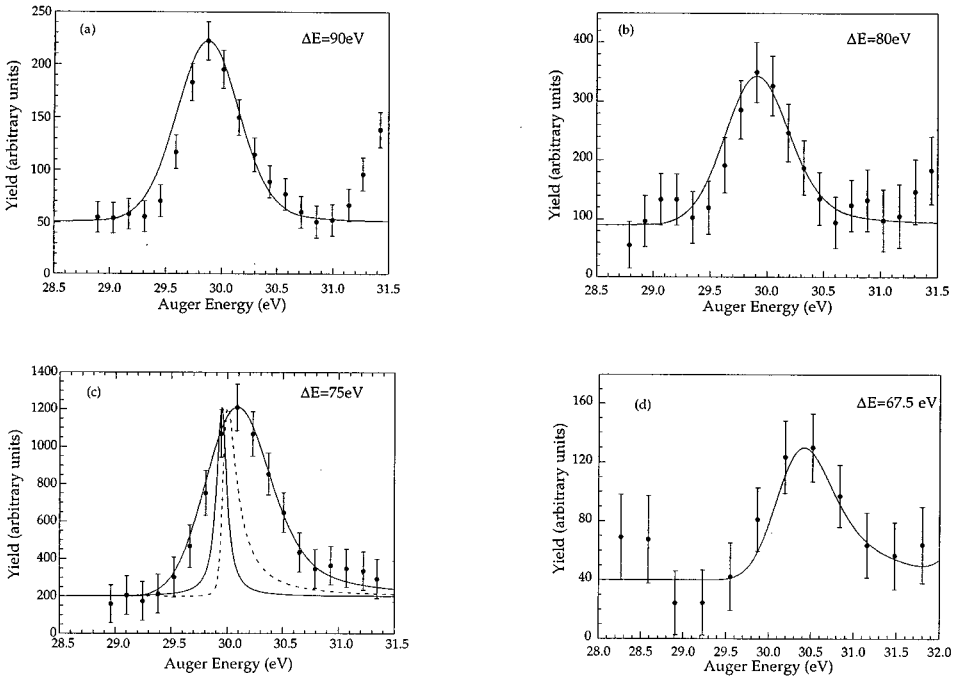

FIG. 8. Xe $N_5O_{23}O_{23}(^1S_0)$ (e,e' Auger) spectra measured at $\Delta E=90$ eV (a), 80 (b), 75 (c), and 67.5 eV (d) compared with the theoretical prediction of the model by Kuchiev and Sheinerman [34] convoluted with the spectrometer response function (full line). As an example of the effect of the convolution procedure the unconvoluted PCI prediction (dashed line) and the Lorentzian line shape of the Auger transition centered at the diagrammatic energy (full line) are shown in Fig. 8(c).

energy-loss experiment of King *et al.* [20], has been used for the natural width of the $4d$ core holes. In order to show the effect of the folding procedure, the Lorentzian line shape of the Auger transition centered at the diagrammatic energy and the theoretical unconvoluted and convoluted line shapes are shown in Fig. 8(c). This figure shows that the effect of the finite energy resolution tends to increase the observed shift, while the overall set of Figs. 8 and 9 proves that the experiment is capable of detecting the variation of the PCI shift with the excess energy. The comparison between experiment and theory is not affected by any adjustable parameter, apart from a scaling factor. The theoretical predictions are in quite good agreement with the $N_5O_{23}O_{23}(^1S_0)$ measurements. Similar agreement is observed in the case of the full spectrum at $\Delta E=90$ eV, while the coincidence spectrum at $\Delta E=67.5$ eV (N_5 threshold), where only the $N_5O_{23}O_{23}$ transitions have been considered, is only poorly reproduced by the theory.

The differences between the PCI calculated spectrum and the experiments observed in Fig. 9(b) have been attributed to the resonant Auger electrons emitted in the decay of the inner-shell excited states because, due to the resolution of the energy-loss channel of the spectrometer ($\approx$1.1 eV FWHM), at $\Delta E=67.5$ eV both the $4d_{5/2}$ state is ionized and the transitions $4d_{3/2}\rightarrow 6p,5d$ and $4d_{5/2}\rightarrow 8p$ may be excited [20]. According the oscillator strengths obtained in the measurements of King *et al.* [20] the $4d_{3/2}\rightarrow 6p$ transition is expected to be the more intense. As discussed in Sec. II the main decay route of these inner-shell excited states is via a resonant Auger process [21] and direct shakeoff of two electrons.

In the shakeoff process the two ejected electrons share in a continuous way the available energy ($\Delta E-I_{\rm ion}^{2+}$), where $I_{\rm ion}^{2+}$ is the double ionization potential of the Xe^{2+} state involved in the process. Considering the first three states of the Xe^{2+} doubly charged ion, at $\Delta E=67.5$ eV the available energy varies from 29.5 to 34 eV. This process can interfere

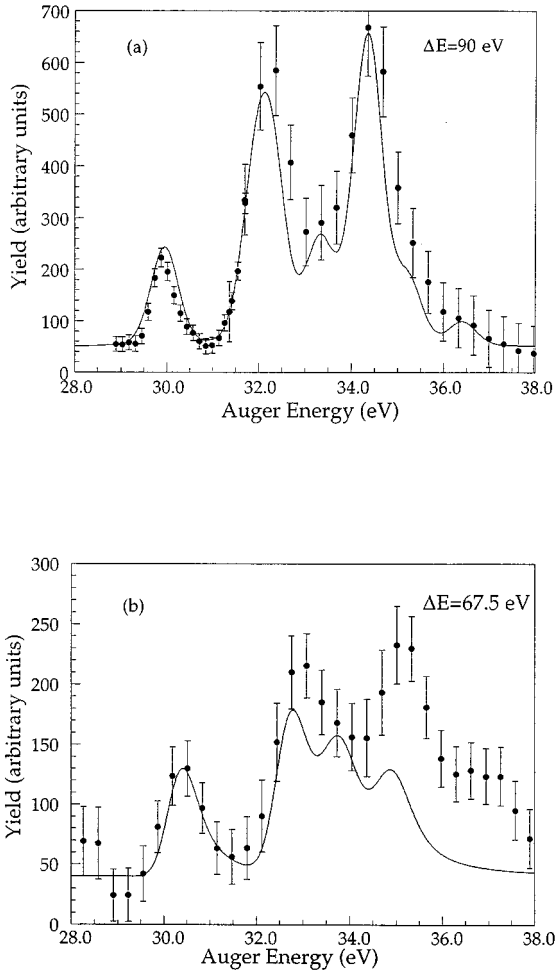

FIG. 9. Xe $N_{45}O_{23}O_{23}$ (e,e' Auger) spectra measured at $\Delta E=90$ eV (a) and 67.5 eV (b) compared with the theoretical prediction of the model by Kuchiev and Sheinerman [34] convoluted with the spectrometer response function (full line).

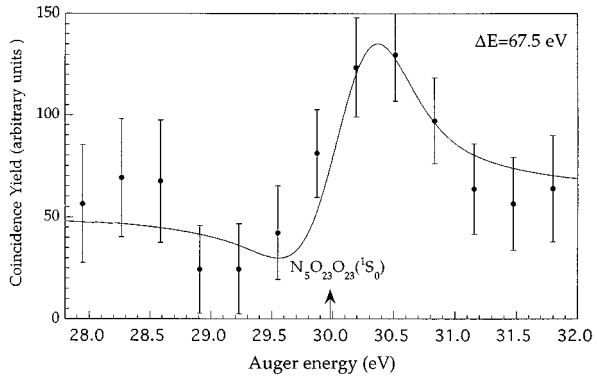

FIG. 10. Xe $N_5O_{23}O_{23}(^1S_0)$ (e,e') Auger) spectra measured at $\Delta E=67.5$ eV. The full line is the fit of the Beutler-Fano line shape to the experiment.

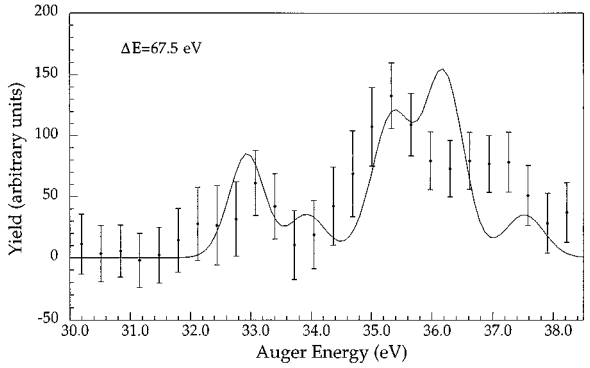

FIG. 11. Difference spectrum between the Xe $N_5O_{23}O_{23}(^1S_0)$ (e,e') Auger) spectra measured at $\Delta E=67.5$ eV and the calculated one of Fig. 8(b). The full line are the experimental data by Ref. [38] convoluted with the energy resolution of the present experiment.

with the Auger decay. The fingerprint of such an interference is always represented by the line shape of the indirect process, which assumes the typical asymmetric profile, known as the Beutler-Fano line shape. The only feature well isolated where the existence of an asymmetric profile can be searched for is the $^1S_0$ peak. As shown in Fig. 10 a Beutler-Fano line shape satisfactorily represents the experimental line shape of the $^1S_0$ transition, proving that the double shakeoff plays a role in the coincidence spectrum taken at $\Delta E=67.5$ eV.

In order to attempt a more quantitative comparison between the present observation and the resonant Auger spectrum recently measured in photon excitation experiments [38] the difference between the experimental spectrum at $\Delta E=67.5$ eV and the predicted one accounting only for the $N_5O_{23}O_{23}$ transitions has been calculated. The comparison of the difference spectrum and the resonant Auger decay spectrum of the $4d_{3/2}^{-1}6p$ state by Aksela *et al.* [38] convoluted with the response function of the coincidence spectrometer is shown in Fig. 11. The region of interest in the present work (32–38 eV) is dominated by the shakeup (d3) transitions. The energy position of the different transitions and their relative intensities have been taken from Table I of Ref. [38] and the comparison is not affected by any adjustable parameter apart from a scaling factor. An overall general agreement is observed between the two spectra. The differences observed may be due to contributions from the decay of the $4d_{3/2}^{-1}5d$ and $4d_{5/2}^{-1}8p$ excited states that occur within the energy resolution of the energy-loss channel of the spectrometer.

The results shown in Figs. 10 and 11 definitely prove that the large discrepancies observed in Fig. 9(b) were due to the excitation of the $4d_{3/2}\rightarrow 6p$ transition by the primary beam and that a significant contribution to the experimental (e,e') Auger) spectrum is due to the resonant Auger processes. Moreover they show that e-e coincidence technique is a suitable tool to investigate the decay of inner-shell excited states. Further support to this statement is given by the results of the further (e,e') Auger) measurement at $\Delta E=65.1$ eV. Within the energy resolution of the energy-loss channel of the spectrometer three transitions can be excited at $\Delta E=65.1$ eV. They are the $4d_{5/2}\rightarrow 6p$, $5d$ and $7p$ transitions. The resonant Auger spectra measured by Aksela *et al.* [38] and Sairanen *et al.* [39] provide information on the energy positions and relative intensities of the peaks in the decay spectrum of the $4d_{5/2}^{-1}6p$ and $7p$ states. The comparison of the present data with the photoexcitation results convoluted with the apparatus function of our spectrometer and with the contribution of the two inner-shell excited states weighted according to a Gaussian function of 1.1 eV FWHM, which represents the resolution of the energy-loss channel, is quite poor. An acceptable representation of the experiment, Fig. 12, is obtained only when other three manifolds of transitions centered at 31.1, 32.6, and 35.3 ± 0.5 eV are taken into account. These contributions may be attributed to the decay of the $4d_{5/2}^{-1}5d$ excited state. A peak corresponding to this optically forbidden transition has been observed to contribute with a small oscillator strength to the energy-loss spectrum measured at 0° by King *et al.* [20]. However the relative strength of such a transition, compared to the other two optically allowed transitions, is expected to increase with the momentum transfer **K**. Thus it is not completely surprising that at $K=0.7$ a.u., the momentum transfer of the present experiment, the decay of the $4d_{5/2}^{-1}5d$ excited state, accounts for ≈40% of the total coincidence yield in the studied region. A tentative assignment of the transition observed might be Xe* $4d_{5/2}^{-1}5d\rightarrow$Xe$+5p^4(^3P)6d$, $(^1D)7p$, and $(^1S)7p$ at

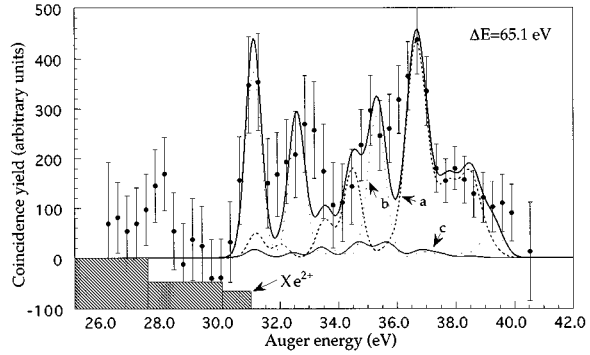

FIG. 12. Xe $(e,e'$Auger) spectra at $\Delta E=65.1$ eV compared with the spectrum of the resonant Auger decay of the $4d_{5/2}^{-1}6p$ (a) and $7p$ (c) states measured in the photoexcitation experiments of Refs. [38] and [39] and convoluted with the energy resolution of the present experiment. Line (b) represents the contribution from the resonant Auger decay of the $4d_{5/2}^{-1}5d$ state and the full line is the sum of all the contributions.

35.3, 32.6, and 31.1 eV respectively. The direct double shakeoff process may explain the coincidence yield observed in the lower-energy side of Fig. 12.

The present energy resolution prevents a definite assignment of the observed features, however, these results show one of the peculiarities of the electron-impact experiments; i.e., they allow one to study optically forbidden transitions and their decay. The study of optically forbidden transitions by electron energy-loss experiments has been pursued since the 1970s [20], but this is the first time that the decay of a state populated via an optically forbidden transition is addressed.

Another process might compete with the resonant Auger decay and produce features in the energy region investigated in the coincidence spectra at $\Delta E=67.5$ and 65.1 eV. This process is the simultaneous ionization and excitation of the Xe valence shells and results in the well-known $5s$ satellite transitions with binding energies between 25 and 45 eV. The $(e,2e)$ processes described by the reaction

$$e(1065.1\leqslant E_0\leqslant 1067.5\ \text{eV})+\text{Xe}\rightarrow \text{Xe}^{+}4d^{10}5s^{2}5p^{4}(^{1}D)nd,ns(^{2}S)+e_a(E_a=1000\ \text{eV})+e_b(20\leqslant E_b\leqslant 43\ \text{eV})$$

would result in a coincidence spectrum with several peaks in the same energy region shown in Figs. 11 and 12. However, the contribution from the satellite states to the measured coincidence spectra is considered negligible because in the $(e,2e)$ satellite spectrum [40] the $5s$ main line is always the stronger feature and a vanishing coincidence yield is measured in the energy region where the $5s$ main line is expected to occur. For example, in the spectrum of Fig. 12, the $5s$ line occurs at 41.7 eV and due to the energy resolution of the spectrometer a rising yield has to be observed already below 40 eV. On the contrary the experiment shows a yield continuously decreasing up to 40 eV. As far as the interpretation is concerned, the satellite spectrum and the resonant Auger can be treated independently. The satellite spectrum is mainly understood in terms of the final ionic state configuration interaction (FISCI) and is dominated by $5s^{2}5p^{4}nd,ns$ electron configurations, while in the resonance decay $5s^{2}5p^{4}np$ configurations are strongly populated. Since the $5s^{2}5p^{4}nd,ns$ configurations have opposite parity as compared to the $5s^{2}5p^{4}np$ ones, mixing via FISCI can not occur.

3. $(e,2e)$ experiments

To compare the observed shifts and line shape of the $(e,2e)$ binding energy spectra with the ones predicted by the PCI models the interaction of the slow ejected electron with all the Auger electrons belonging to the $N_{45}OO$ transition manifold has to be accounted for. In the present calculations we have accounted for the Auger lines that correspond to the Xe^{2+} $5p^{4}$, $5s5p^{5}$, and $5s^{0}$ final states. The contribution of the different transitions has been weighted according the relative intensities determined in the electron-impact experiment by Aksela, Aksela, and Pulkkinem [32]. The theoretical line shapes have been then convoluted with the spectrometer response function. The shifts calculated at $\Delta E=90$, 80, and 75 eV are 0.04, 0.12, and 0.21 eV, respectively, while the asymmetric broadening of the line shape as ΔE decreases results in a FWHM that is ≈10% larger than the expected FWHM from the apparatus function at $\Delta E=75$ eV. The calculated shifts and line shapes are consistent with the experimental observations, although at the smaller ΔE the calculations predict smaller values than the observed ones.

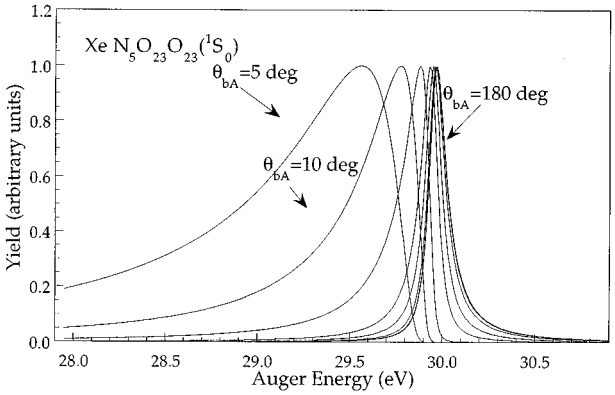

FIG. 13. Xe $N_5O_{23}O_{23}(^1S_0)$ line shapes calculated according the model of Kuchiev and Sheinerman [34] for various relative angle between the Auger and ejected electrons.

4. $(e,e'$ Auger) experiments: PCI angular dependence

Kuchiev and Sheinerman's model, as well as all the nonisotropic PCI theories, predict an angular dependence of the PCI effects. This mainly arises by the interaction between the slow ejected and Auger electrons. In Fig. 13 the line shapes, calculated according the model of Kuchiev and Sheinerman [34] for several ϑ_{bA} values from 180° and 5° are shown. A progressive change from a small positive shift with respect to the diagrammatic position of the $N_5O_{23}O_{23}(^1S_0)$ Auger transition and an asymmetric high-energy flank of the peak to a negative shift with a large asymmetry on the low-energy side is observed.

In order to compare the calculated PCI line shape with the experiment, the theoretical predictions have to be convoluted with the energy and angular response functions of the spectrometer. The energy response function has been determined from the noncoincidence Auger measurements, while the angular response function has been obtained by a computer simulation of the trajectories transmitted by the lens stack and the following dispersing element. The knowledge of this function is quite important at $\vartheta_{bA}=25°$, because the theoretical PCI line shapes suffer substantial variations when ϑ_{bA} varies from 20° to 30°. By applying the convolution procedure to the same line shapes of Fig. 13 it has been ascertained that the experiment was able to detect and distinguish the expected shifts at the two angles where the measurements were done. The comparison between the theoretical predictions and the experiment is shown in Fig. 14. A satisfactory agreement between theory and experiment is observed in both the measured cases, although at $\vartheta_{bA}=25°$ the experiment seems to indicate a shift slightly larger than the theory. This difference may be attributed to the theoretical assumption of rectilinear trajectories for the unbound electrons. In-

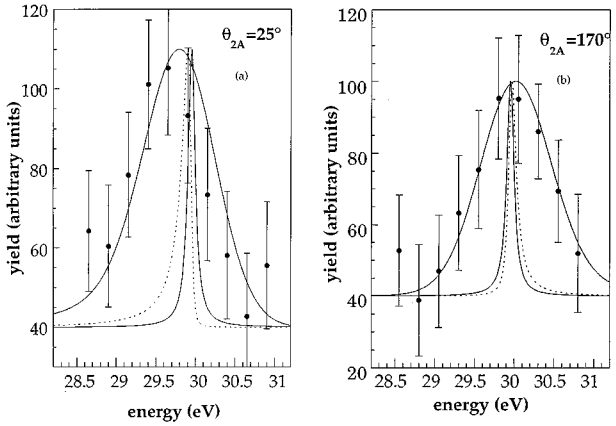

FIG. 14. The coincidence (dots) spectra of the Xe $N_5O_{23}O_{23}(^1S_0)$ Auger line at 1000-eV incident energy and $\vartheta_{bA}=25°$ ($\vartheta_b=15°$ and $\vartheta_A=40°$) (a) and 170° ($\vartheta_b=260°$ and $\vartheta_A=90°$) (b) compared with the convoluted PCI line shapes (full line) [34]. In the figures also the Lorentzian [full line centered at 29.95, i.e., the diagrammatic energy of the $N_5O_{23}O_{23}(^1S_0)$ Auger line] and unconvoluted (dashed line) are shown.

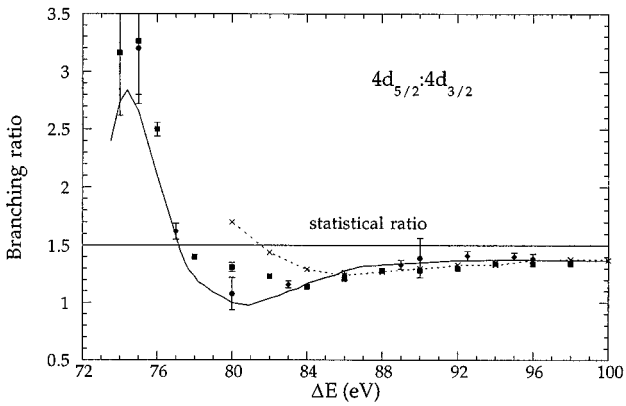

FIG. 15. Xe $4d$ branching ratio vs ΔE. The present results (dots) and the experiments by Yates *et al.* [42] (squares) and Ausmees *et al.* [43] (diamonds) are compared with RRPA calculations by Cheng and Johnson [47] (full line) and Johnson and Cheng [50] (dashed line with crosses).

deed $(e,2e)$ studies [41] have shown that, due to their mutual interaction, free electrons of kinetic energy as high as 100 eV suffer a displacement of few degrees from their original trajectory.

B. $4d_{5/2}$:$4d_{3/2}$ branching ratios

In order to interpret the observed variation of the branching ratio we have to recall that these $(e,2e)$ experiments have been performed with a procedure that mimics a photoionization experiment at fixed $h\nu$. Yates *et al.* [42] and Ausmees *et al.* [43] have measured the $4d$ branching ratio from 74 to 250 eV in photoelectron experiments and observed a similar variation. A comparison between the present $(e,2e)$ data and the photoionization results is shown in Fig. 15. Good agreement within the experimental uncertainties is observed between the different sets of data, independently from the type of the experiment.

Similar variations of the branching ratio were also observed in the Xe $5p$ photoemission experiments [44,45]. Walker and Waber [46] already in 1974 interpreted this variation as a result of the small but significant differences in the two bound state wave functions and of the differences in the kinetic energy of the photoelectrons produced at a fixed $h\nu$. They qualitatively stated that where the cross section was rising the ratio would be greater than the statistical one, while it would be less than the statistical in the region of falling cross section. After this explanation a better understanding of the photoionization data has been reached only via the relativistic random phase approximation (RRPA) calculations [47–50]. In Fig. 14 the RRPA calculation of Cheng and Johnson [47], performed in intermediate coupling using six interacting channels, is represented by the full line. The agreement of this calculation with the global set of experimental data is satisfactory, although some differences are observed in the region of the minimum. Recently new calculations of the $4d$ partial photoionization cross sections have been performed including the core relaxation [49] and the coupling between channels from other subshells [50]. As shown in the figure the RRPA calculation with the inclusion of the relaxation (dashed line with crosses) considerably overestimates the measured branching ratio in the region below 85 eV, while it is in good agreement with the experiments and previous RRPA calculations [47] at higher energy. This shows that the region closer to threshold is the more sensitive one to test the ability of the model to account correctly for intrashell and intershell coupling, relaxation processes, and photoelectron dynamics.

Once we understood the reason for the variation of the $4d$ branching ratio, it was interesting to note that despite the quite large momentum transfer ($K\approx0.7$ a.u.) of the present $(e,2e)$ experiments, which in the case of $\Delta E=75$ eV matches the conditions for an impulsive collision [4], their results are consistent with photoionization data, while the $(e,2e)$ angular distributions measured upon the same kinematics are quite far from the dipolar ones expected for the photoelectrons [13]. This finding shows that the $(e,2e)$ angular distributions are very sensitive to the details of the ionization mechanism. Indeed the angular distributions of the photoelectrons, in the nonrelativistic regime, can be described in terms of only one parameter, the asymmetry parameter β, evaluated on the ground of the dipole selection rules and of the radial matrix elements. On the contrary, the $(e,2e)$ angular distributions can never be described in terms of a pure dipolar matrix element, even at incident energy as high as 8000 eV and $K\leqslant0.1$ a.u [51]. Moreover, final-state interactions in the continuum between the unbound electrons add further complexity to the electron-impact ionization.

VI. CONCLUSIONS

An electron-impact coincidence apparatus, equipped with three different electrostatic analyzers, has been used to tackle the simultaneous investigation of the Xe $4d$ excitation and ionization and decay.

The physical effect that dominates the energy region investigated, i.e., near threshold, is the PCI among the unbound electrons in the final state. In this work a complete study of PCI has been performed by the simultaneous observations of the final-state effects in the ionizing and decay

channels and by the observation of the PCI angular dependence in an electron-impact experiment. This latter observation shows the importance of treating on an equal footing all the interactions [electron(s)-electron(s) and electron(s)-ion interactions] in the final state of an ionization event induced by charged-particle impact. This is a well-known fact in the study of the ionization mechanism of the outer shell by electron impact, but its relevance to PCI effects has been neglected until the late 1980s, i.e., after more than 20 years from their first observation [52]. As far as the comparison with the theory is concerned, the actual PCI models, despite some crude assumptions such as the rectilinear trajectories of the escaping electrons, give a satisfactory description of the shift and the change of the Auger line shape.

The results obtained for the decay of the inner-shell excited states and for the $4d$ branching ratio, compared with photoionization results, show that electron-impact coincidence experiments are a viable method to study these problems. Electron-impact studies, in addition, give the possibility to study the excitation and decay of dipole forbidden transitions, as shown in this work in the case of the Xe* $4d_{5/2}^{-1}5d$. Moreover due to the limited availability of beam time at the third-generation synchrotron radiation facilities electron-impact studies become essential in identifying particular problems for detailed study and in developing the experimental and computational methods needed.

As far as the experimental method is concerned, this work has shown that the electron-electron coincidence techniques are very effective in the study of the finer details of inner-shell processes. A clear example is given by the coincidence line shape of the $N_5O_{23}O_{23}(^1S_0)$ Auger transition measured at $\Delta E=67.5$ eV, where the competition between the direct double ionization and the two-step decay resulted in an asymmetric Beutler-Fano profile. The main limit of this technique is still the long accumulation time needed to achieve an acceptable statistics. The experimental challenge for the future consists in developing new experimental apparatuses that allow one to collect events from the largest possible fraction of the total solid angle, without losing detailed directional information [53–56].

ACKNOWLEDGMENT

This work was partially supported by EEC Contract No. CHRX-CT93-0350 and by NATO CRG No. 920101.

[1] H. Ehrhardt, G. Knoth, P. Schlemmer, and K. Jung, Z. Phys. D **1**, 3 (1986).

[2] L. Avaldi, R. Camilloni, E. Fainelli, and G. Stefani, in *The Physics of Electronic and Atomic Collisions*, edited by W. R. MacGillivray, I. E. McCarthy, and M. C. Standage (Adam Hilger, Bristol, 1992), p. 219.

[3] C. T. Whelan, R. J. Allan, H. R. J. Walters, and X. Zhang, in (*e*,2*e*) *& Related Processes*, edited by C. T. Whelan *et al.* (Kluwer Academic, Dordrecht, 1993), p. 33.

[4] L. Avaldi, R. Camilloni, E. Fainelli, and G. Stefani, J. Phys. B **20**, 4163 (1987).

[5] C. B. Brion, in *The Physics of Electronic and Atomic Collisions*, edited by T. Andersen *et al.*, AIP Conf. Proc. No. 295 (AIP, New York, 1993), p. 350.

[6] G. Stefani, L. Avaldi, and R. Camilloni, J. Phys. B **23**, L227 (1990).

[7] C. Dupre', A. Lahmam-Bennani, A. Duguet, F. Mota-Furtado, P. F. O'Mahony, and C. Dal Cappello, J. Phys. B **25**, 259 (1992).

[8] L. Avaldi, R. Camilloni, G. C. King, and G. Stefani, Phys. Rev. A **44**, 4740 (1991).

[9] R. Camilloni, A. Giardini-Guidoni, R. Tiribelli, and G. Stefani, Phys. Rev. Lett. **29**, 618 (1972).

[10] A. Lahmam-Bennani, H. F. Wellestein, A. Duguet, and A. Daoud, Phys. Rev. A **30**, 1511 (1984).

[11] L. Avaldi, R. Camilloni, and G. Stefani, Phys. Rev. A **41**, 134 (1990).

[12] P. Bickert, W. Hink, C. DalCappello, and A. Lahmam-Bennani, J. Phys. B **24**, 4603 (1991).

[13] L. Avaldi, R. Camilloni, R. Multari, G. Stefani, X. Zhang, H. R. J. Walters, and C. T. Whelan, Phys. Rev. A **48**, 1195 (1993).

[14] E. C. Sewell and A. Crowe, J. Phys. B **17**, 2913 (1984).

[15] W. Sandner and M. Völkel, J. Phys. B **17**, L597 (1984).

[16] G. Stefani, L. Avaldi, A. Lahmam-Bennani, and A. Duguet, J. Phys. B **19**, 3787 (1986).

[17] B. Lohmann, J. Phys. B **24**, L249 (1991).

[18] U. Becker, D. Szostak, H. G. Kerkhoff, H. Kupsch, B. Langer, R. Whelitz, A. Yagishita, and T. Hayaishi, Phys. Rev. A **39**, 3902 (1989).

[19] K. Okuyama, J. H. D. Eland, and K. Kimura, Phys. Rev. A **41**, 4930 (1990).

[20] G. C. King, M. Tronc, F. H. Read, and R. C. Brandford, J. Phys. B **10**, 2479 (1977).

[21] U. Becker, T. Prescher, E. Schmidt, B. Sonntag, and H. E. Wetzel, Phys. Rev. A **33**, 3891 (1986).

[22] For a review see V. Schmidt, Rep. Prog. Phys. **55**, 1483 (1992), and references therein.

[23] M. Schnetz and W. Sandner, in *Proceedings of the Conference on Correlation and Polarization in Electronic and Atomic Collisions and* (*e*,2*e*) *Reactions*, IOP Conf. Proc. No. 122, edited by P. J. O. Teubner and E. Weigold (Institute of Physics, Bristol, 1992), p. 139.

[24] B. Lohmann, X.-K. Meng, and M. Keane, J. Phys. B **25**, 5223 (1992).

[25] B. Kammerling, B. Krassig, and V. Schmidt, J. Phys. B **26**, 261 (1993).

[26] L. Sarkadi, T. Vajnai, J. Vegh, and A. Kover, J. Phys. B **24**, 1655 (1991).

[27] L. Avaldi, P. Belotti, P. Bolognesi, R. Camilloni, and G. Stefani, Phys. Rev. Lett. **75**, 1915 (1995).

[28] R. Dutil and P. Marmet, Int. J. Mass Spectrom. Ion Phys. **35**, 371 (1980).

[29] T. Hayaishi, Y. Morioka, Y. Kageyama, M. Watanabe, I. H. Suzuki, A. Mikuni, G. Isoyama, S. Asooka, and M. Nakamura, J. Phys. B **17**, 3511 (1984).

[30] Von Raven, M. Meyer, M. Pahler, and B. Sonntag, J. Electron. Spectrosc. Relat. Phenom. **52**, 677 (1990).
[31] E. Fainelli, R. Camilloni, G. Petrocelli, and G. Stefani, Nuovo Cimento D **9**, 33 (1987).
[32] H. Aksela, S. Aksela, and H. Pulkkinem, Phys. Rev. A **30**, 865 (1984).
[33] P. van der Straten, R. Mongerstern, and A. Niehaus, Z. Phys. D **8**, 35 (1988).
[34] M. Yu. Kuchiev and S. A. Sheinerman, Usp. Fiz. Nauk **158**, 353 (1989) [Sov. Phys. Usp. **32**, 569 (1989)].
[35] G. B. Armen, J. Tulkki, T. Aberg, and B. Crasemann, Phys. Rev. A **36**, 5606 (1987).
[36] A. Russek and W. Mehlhorn, J. Phys. B **19**, 911 (1986).
[37] M. Inokuti, Rev. Mod. Phys. **43**, 297 (1971).
[38] H. Aksela, O.-P. Sairanem, S. Aksela, A. Kivimäki, A. Naves de Brito, and E. Nõmmiste, Phys. Rev. A **51**, 1291 (1995).
[39] O.-P. Sairanen, H. Aksela, S. Aksela, J. Mursu, S. T. Osborne, A. Ausmees, and S. Svensson, J. Phys. B **28**, 4509 (1995).
[40] S. Braidwood, M. Brunger, and E. Weigold, Phys. Rev. A **47**, 2927 (1993).
[41] L. Avaldi, R. Camilloni, Yu. V. Popov, and G. Stefani, Phys. Rev. A **33**, 851 (1986).
[42] B. W. Yates, K. H. Tan, L. L. Coatsworth, and G. M. Bancroft, Phys. Rev. A **31**, 1529 (1985).
[43] A. Ausmees, S. J. Osborne, R. Moberg, S. Svensson, S. Aksela, O.-P. Sairanem, A. Kivimäki, A. Naves de Brito, E. Nõmmiste, J. Jauhiinem, and H. Aksela, Phys. Rev. A **51**, 855 (1995).
[44] H. J. Levinson, I. T. McGovern, and T. Gustafsson, J. Phys. B **13**, 253 (1980).
[45] M. O. Krause, T. A. Carlson, and P. R. Woodruff, Phys. Rev. A **24**, 1374 (1981).
[46] T. E. H. Walker and J. T. Waber, J. Phys. B **7**, 674 (1974).
[47] K. T. Cheng and W. R. Johnson, Phys. Rev. A **28**, 2830 (1983).
[48] N. Shanti and P. C. Desmukh Phys. Rev. A **40**, 2400 (1989).
[49] M. Kutzner, V. Radojevic, and H. P Kelly, Phys. Rev. A **40**, 5052 (1989).
[50] W. R. Johnson and K. T. Cheng, Phys. Rev. A **46**, 2952 (1992).
[51] M. Zitnik, L. Avaldi, R. Camilloni, and G. Stefani, J. Phys. B **27**, L851 (1993).
[52] R. B. Barker and H. W. Berry, Phys. Rev. **151**, 14 (1966).
[53] B. R. Todd, N. Lermer, and C. E. Brion, Rev. Sci. Instrum. **65**, 977 (1994).
[54] M. J. Ford, J. P. Doering, M. A. Coplan, J. W. Cooper, and J. H. Moore, Phys. Rev. A **51**, 418 (1995).
[55] M. Zitnik, A. Kover, D. Dilena, L. Avaldi, R. Camilloni, M. deSimone, E. Paiser, L. Frost, and G. Stefani (unpublished).
[56] R. Whelitz, J. Viefhaus, K. Wieliczek, B. Langer, S. B. Whitfield, and U. Becker, Nucl. Instrum. Methods B **99**, 257 (1995).
[57] J. E. Hansen and W. Persson, Phys. Rev. A **18**, 1459 (1978).
[58] J. E. Hansen and W. Persson, Phys. Scr. **25**, 487 (1981).